Vertical Wind Shear Associated with Left-Moving Supercells

MATTHEW J. BUNKERS

NOAA/NWS Weather Forecast Office, Rapid City, South Dakota

(Manuscript received 6 September 2001, in final form 21 February 2002)

ABSTRACT

Vertical wind shear parameters are presented for 60 left-moving supercells across the United States, 53 of which produced severe hail (≥1.9 cm). Hodographs corresponding to environments of left-moving supercells have a tendency to be more linear than those of their right-moving supercell counterparts. When curvature is present in the hodographs of the left-moving supercells, it is typically confined to the lowest 0.5–1 km. Values of 0–6-km wind shear for left-moving supercells—both bulk and cumulative—are within the ranges commonly found in right-moving supercell environments, but the shear values do occur toward the lower end of the spectrum. Conversely, the absolute values of storm-relative helicity (SRH) for left-moving supercells are much smaller, on average, than what occur for right-moving supercells (although SRH values for many right-moving supercells also fall well below general guidelines for mesocyclone development). A significant fraction of the 0–3-km SRH (25%) and 0–1-km SRH (65%) for left-moving supercells is positive, owing to the shallow clockwise curvature of the hodographs. However, nearly all of the 1–3-km SRH for left-moving supercells is negative, with absolute values comparable in magnitude to those for right-moving supercells. A limited climatological analysis of vertical wind shear associated with convective environments across parts of the central United States suggests that clockwise curvature of the low-level shear vector is most common in the central/southern plains, partially explaining the preeminence of right-moving supercells in that area. In contrast, hodographs are more linear over the northern high plains, suggesting left-moving supercells may be relatively more common there. It would be beneficial to implement operational radar algorithms that can detect mesoanticyclones across the United States.

1. Introduction

A review of the meteorological literature indicates that left-moving[1] supercells have not been documented as frequently as right-moving supercells across the United States. This may be due in part to their relative infrequency, or perhaps it is because left-moving supercells are rarely known to produce tornadoes. Although extensive documentation is not readily available, left-moving supercells are recognized operationally as large-hail producers, and furthermore, they may persist for several hours in certain environments (e.g., Achtemeier 1969; Charba and Sasaki 1971; Matthews and Turnage 2000).

Assuming horizontally homogeneous conditions, numerical model simulations suggest that both left- and right-moving supercells are equally favorable in a unidirectionally sheared environment, with left-movers (right movers) increasingly favored when the low-level shear vectors turn counterclockwise (clockwise) with height and the shear strengthens (Weisman and Klemp 1986; Weisman and Rotunno 2000). These modeling results have been supported by some observational studies (e.g., Burgess and Curran 1985; Nielsen-Gammon and Read 1995; Scarlett 1998). Furthermore, a limited sample of left-moving supercells across Australia also revealed counterclockwise curvature in the lowest few kilometers of the composite hodograph (Dickins 1994).

Other studies, however, have highlighted examples where left-moving supercells have been long lived, even though the shear vectors exhibited clockwise curvature in the lowest few kilometers of the hodograph (e.g., McCann 1983; Grasso and Hilgendorf 2001)—a condition presumed to be detrimental to the persistence of left-moving supercells. Possible explanations for the longevity of left-moving supercells in environments with clockwise curvature of the low-level shear vectors are (i) convergence along the gust front of the storm (Wilhelmson and Klemp 1981; Brown and Meitín 1994), (ii) strong low-level storm-relative inflow of positively

[1] Left-moving supercells are herein defined as supercells exhibiting clockwise rotation that travel to the left of the vertical wind shear vector, and right-moving supercells are defined as supercells with counterclockwise rotation that travel to the right of the vertical wind shear. This definition is more consistent with supercell dynamics than one that uses the mean tropospheric wind as a reference (e.g., Weisman and Klemp 1986; Weisman and Rotunno 2000).

Corresponding author address: Matthew J. Bunkers, NOAA/NWS Weather Forecast Office, 300 E. Signal Dr., Rapid City, SD 57701-3800.
E-mail: matthew.bunkers@noaa.gov

buoyant air (e.g., Grasso 2000), and (iii) hodograph curvature confined to the lowest 1 km (discussed in section 4 below). Numerical simulations, presented in Weisman and Klemp (1986, their Fig. 15.17C), revealed a left-moving supercell that persisted for about an hour when low-level clockwise curvature was present, although it was less intense than the right-moving supercell.

The occurrence of left-moving supercells in kinematic environments that appear initially unfavorable for their development has led to some confusion, especially regarding the prediction of their intensity and longevity. Some of this confusion has arisen because observations of the kinematic environments of left-moving supercells are not well documented—with a relatively limited number of case studies of left-moving supercells present in the literature. Therefore, in an attempt to better understand the vertical wind shear associated with left-moving supercells, kinematic sounding data from the environments of 60 left-moving supercells across the United States were investigated. The primary objective of this research was to determine similarities and differences among shear-related parameters for left- and right-moving supercells, with an emphasis on operational forecasting. Based on the literature cited above, it was expected that the vertical wind shear magnitude would be similar for all supercell environments, but both the degree and depth of turning of the shear vectors[2] would be different depending on whether left- or right-moving supercells were dominant.

2. Data and methods

a. Supercell data

Left-moving supercell hodographs and motions were gathered in a manner consistent with the methods described in Bunkers et al. (2000). Thirty-six of the 60 cases were obtained across the central United States using the Weather Surveillance Radar-1988 Doppler (WSR-88D) archived data. The remaining 24 cases resulted from a search through the meteorological literature, with many of the events documented in Brown and Meitín (1994), and the others contained in Fankhauser (1971), Knupp and Cotton (1982), Andra (1993), Kleyla (1993), Phillips (1994), Nielsen-Gammon and Read (1995), Stuart (1997), Matthews and Turnage (2000), Monteverdi et al. (2001), and Weaver et al. (2001). There are a few other examples of left-moving supercells in the meteorological literature, but they were not included in the present dataset because the sounding data were deemed unrepresentative (e.g., Grasso and Hilgendorf 2001). Furthermore, there may be some cases in the present dataset where the synoptic-scale sounding did not capture the true wind profile of the left-moving supercell event, so some skepticism is warranted when viewing the results.

TABLE 1. Total number of hodographs associated with left- and right-moving supercells, number of hodographs contained in both datasets, and number of cases with both left- and right-moving supercells present.

Hodograph designation	Total No. of hodographs	No. of hodographs double counted	No. of events with supercells of both type present
Right-mover	479	43	50–100 (estimated)
Left-mover	60	43	48

In addition, a dataset of 479 right-moving supercells (some tornadic, some nontornadic) was developed for comparison of the shear-related parameters with the left-moving supercell dataset. These data consisted of (i) the 260 right-moving supercells from Bunkers et al. (2000), (ii) an additional 194 cases collected across the central United States using the WSR-88D archived data, and (iii) 25 cases provided by Edwards and Thompson (2000). All necessary observed sounding data were retrieved either from the National Climatic Data Center (NCDC) *Radiosonde Data of North America 1946–1997* CD-ROMs or from the online archive provided by the Forecast Systems Laboratory (FSL) for post-1997 data (http://raob.fsl.noaa.gov). Because of the unavailability of observed soundings in some instances (i.e., the storm was not close in time/space to a sounding site), Rapid Update Cycle (RUC) analysis soundings were utilized for 17 of the right-moving supercell cases in 2001. Thompson and Edwards (2000) found that RUC analysis soundings were reasonably representative of observed soundings at the same locations, and that they were fairly reliable for deep-layer vertical wind shear parameters. Moreover, Hamill and Church (2000) used RUC analysis and forecast data to determine whether relationships existed between gridded model data and observed severe weather reports, and their results compared favorably with previous radiosonde-based studies. All sounding wind data were interpolated to 0.5-km increments from the surface to 8 km.

There are 43 hodographs that are not unique to either dataset; thus, the hodograph datasets are not mutually exclusive (Table 1). This occurred because for 48 of the left-moving supercell events, right-moving supercells were also present. Data for both supercells were then gathered if the storms were relatively isolated and both the space and time constraints, referenced above, were met for each of the storms. It is unknown how often left-moving supercells occurred for each event in the right-moving supercell dataset, but this number is expected to be relatively small [e.g., 10%–20%; R. Thompson (2001, personal communication)]. However, one must keep in mind that most of the hodographs in the left-moving supercell dataset were also associated with right-moving supercells (and this is indicated in

[2] Operationally, curvature of a hodograph is often taken to mean both the turning of the shear vectors plus the depth over which they turn.

the figures that follow). Furthermore, it is apparently rare for left-moving supercells to occur in the United States without a right-moving supercell counterpart (12 of 60 = 20% of the events).

Information on severe hail (≥1.9 cm; larger than dimes) was also obtained, if it occurred, for the 60 left-moving supercells. These data were available from the (i) historical severe weather report database using the software of Hart and Janish (1999), (ii) daily severe storm reports from the Storm Prediction Center, or (iii) meteorological literature cited above. Fifty-three of the 60 supercells (nearly 90%) produced at least 1.9-cm hail at some point during their lifetime. Moreover, the mean, median, and modal hail sizes corresponding to the 53 severe hail reports were all 4.4 cm (golfball size). This corroborates the notion that both left- and right-moving supercells often produce large hail, and is consistent with the results of Burgess and Lemon (1991), who noted that 30 of 32 supercells with mesocyclones (94%) produced some form of severe weather during their lifetime. The occurrence of severe wind gusts and tornadoes with left-moving supercells was not addressed in the present study.

b. Analysis methods

In light of the numerical model simulations previously mentioned, the hodographs for the left-moving supercells were partitioned based upon the degree of shear vector turning in the lowest 3 km. If the shear vectors turned clockwise by 45° or more through at least 1 km, and up to 3 km, the hodograph was classified as clockwise-curved; otherwise, if the hodograph exhibited less clockwise turning of the shear vectors than 45° in the lowest 3 km, *or if the curvature was only confined to the lowest 0.5 km of the atmosphere,* the hodograph was classified as straight. Based on this analysis method, 22 of the 60 hodographs (37%) were classified as clockwise-curved while the remaining 38 (63%) exhibited predominantly unidirectional shear, or slight counterclockwise curvature. Only four hodographs had significant counterclockwise curvature in the lowest 0.5 km. Moreover, of the 22 clockwise-curved hodographs, eight of them (36%) displayed curvature only through the lowest 1 km of the atmosphere. Even though most of the left-moving supercell hodographs were characterized by linear shear as defined above, clockwise turning of the shear vectors of 90° or more was present through the lowest 2–3 km of the hodographs for 10 of the 60 cases (17%).

The 0–6-km wind shear was calculated using two different techniques. First, the 0–6-km bulk wind shear is represented by the vector difference between the surface and 6-km winds. It has the same units as the square root of the bulk Richardson number (BRN) shear term (Weisman and Klemp 1986; Droegemeier et al. 1993), but is often larger. Second, the 0–6-km total (also called cumulative) wind shear [similar to mean shear; Rasmussen and Wilhelmson (1983)] is represented by a summation of the shear segments across each 0.5-km sublayer from 0 to 6 km. This is a measure of hodograph length, and is analogous to ''stretching out'' the hodograph and calculating the bulk shear. For a purely unidirectional hodograph that does not fold back on itself, the bulk shear and total shear must be equal; and for a curved hodograph, the bulk shear will always be less than the total shear, often times by a factor of 2 (as seen in the present dataset).

Storm-relative helicity (SRH) was calculated for the 0–3-, 0–1-, and 1–3-km layers using the observed storm motions and the equation presented in Davies-Jones et al. (1990). The mean wind in the 0–1-km layer was also used to calculate the low-level storm-relative inflow. It is important to note that the magnitudes of deep-layer shear and SRH are dependent upon the vertical sampling interval (e.g., Markowski et al. 1998a), which is 0.5 km in the present study.

In order to emphasize the relative differences between environments, composite hodographs were developed for the left- and right-moving supercells by (i) translating the origin of the hodograph to the point defined by the 0–0.5-km mean wind, (ii) rotating the hodograph such that the 0–6-km wind shear was positive and parallel to the abscissa, (iii) averaging the components of the wind as a function of height, and (iv) averaging the components of the storm motion. This technique is a modification of that presented in Rasmussen and Straka (1998). Three composite hodographs were produced: (i) one for the 12 left-moving supercells with no associated right-moving supercells (hereinafter denoted as LM-only); (ii) one for the remaining 48 left-moving supercells, which also had right-moving supercells in the same environment (hereinafter denoted as LM–RM); and (iii) one for the 479 right-moving supercells that also had left-moving supercells in the same environment for an estimated 10%–20% of the cases (hereinafter denoted as RM). This simpler compositing procedure was selected in favor over that of Brown (1993) because of the size of the datasets. Furthermore, the present technique places the greatest emphasis on the lowest 1–3 km of the hodograph, which is where the primary differences between the left- and right-moving supercell hodographs exist.

Last, in order to perform a limited climatological analysis, all observed soundings were collected for the period 1948–2000 from four sites in the northern high plains (NHP: Rapid City, South Dakota; Bismarck, North Dakota; Glasgow, Montana; Great Falls, Montana) and from four sites in the central/southern plains (CSP: Springfield, Missouri; Topeka, Kansas; Norman, Oklahoma; Fort Worth, Texas). Furthermore, only those hodographs associated with environments capable of producing deep moist convection were analyzed. Chosen thresholds were surface-based convective available potential energy (SBCAPE) > 50 J kg^{-1} and convective inhibition (SBCIN) < 50 J kg^{-1} [using the virtual tem-

perature correction described in Doswell and Rasmussen (1994)]. Forecast storm motions for both left- and right-moving supercells were estimated using the shear-relative method presented in Bunkers et al. (2000), thereby allowing computation of the 0–3-km forecast SRH (hereinafter denoted as SRH_f).

3. Results

a. Composite hodographs for supercell environments

Composite hodographs for the left- and right-moving supercells illustrate important differences, especially between the LM-only and RM partitions (Fig. 1). First, the composite hodograph for the LM-only partition is essentially unidirectional, albeit there is slight counterclockwise turning of the shear vectors in the lowest 1 km and also from 3 to 5 km (Fig. 1a). In the case of the LM–RM partition, clockwise turning of the shear vectors is evident in the lowest 1 km of the composite hodograph, followed by a gradual counterclockwise turning of the shear vectors through 1–7 km (Fig. 1b). For the composite hodograph corresponding to the RM partition, the shear vectors turn clockwise through the lowest 2 km, while the 2–8-km layer displays little curvature (Fig. 1c)—similar to the composites of Maddox (1976) and Brown (1993). It is apparent that counterclockwise-curved hodographs are not common in supercell environments across the United States.

The LM-only composite hodograph is clearly distinguishable from the LM–RM and RM composites in the lower atmosphere by virtue of the curvature of the shear vectors (Fig. 1). The vertical wind shear is also weaker throughout the hodograph for the LM-only partition, especially in the lowest 2 km (Table 2, leftmost columns). Conversely, the differences between the LM–RM and RM composite hodographs are more subtle: (i) only the depth of the clockwise curvature is greater for the RM composite hodograph, which leads to slightly stronger low-level storm-relative flow (and larger SRH), and (ii) the vertical wind shear in the 2–8-km layer is greater for the LM–RM composite hodograph, leading to stronger storm-relative flow at 8 km (Table 2). It is also worth noting that both the LM-only and LM–RM composite hodographs are similar in displaying a greater degree and depth of turning of the shear vectors in the midlevels; however, the LM–RM and RM composite hodographs are both alike in having stronger upper-level winds (both ground and storm relative). Assuming a left-moving supercell was associated with the RM composite hodograph, the 0–3-km SRH_f would be $-27\ m^2\ s^{-2}$ (cf. with the observed values for the LM-only and LM–RM partitions in Table 2). If the hodograph compositing procedure of Brown (1993) had been used in this analysis, the differences in Fig. 1 likely would have been more pronounced [e.g., see the comparison in Dickins (1994)]. In summary, the clockwise turning of the low-level shear vectors occurs over a deeper layer for the RM composite hodograph when compared with the LM–RM composite, and the shear vectors show a slight counterclockwise turning for the LM-only composite.

b. Vertical wind shear for supercell environments

A consistent pattern exists in both the 0–6-km bulk and total wind shear for the two supercell datasets (Fig. 2). In general, supercell processes are very rare when the 0–6-km bulk (total) wind shear is $<10\ m\ s^{-1}$ ($<20\ m\ s^{-1}$)—as noted in reference to the solid lines in Fig. 2. As a reference, the climatological minimum values of the 0–6-km bulk (total) shear for the NHP and CSP regions are around $1\ m\ s^{-1}$ (8–10 m s^{-1}). Ninety-five percent of all supercells were associated with 0–6-km bulk (total) wind shear $>13\ m\ s^{-1}$ ($>25\ m\ s^{-1}$). Also note that the total vertical wind shear is often 1.5–2 times greater than the bulk shear. These results are consistent with numerical model simulations of supercells, which establish a lower threshold of 0–6-km total wind shear of about 20–25 m s^{-1} (e.g., UCAR 1996).

The maximum 0–6-km shear values for the left-moving supercells are 10–20 m s^{-1} less than those for right-moving supercells (cf. Figs. 2a and 2b). This might be attributable to the much smaller dataset of left-moving supercells. Indeed, the 95th percentile values of the 0–6-km bulk and total wind shear for the right-moving supercell dataset are 37 and 59 m s^{-1}, respectively, which compare well with the maximums for the left-moving supercells. Therefore, as more observations of left-moving supercells accumulate, it should not be surprising to see slightly larger maximum values of vertical wind shear.

Interestingly, the 0–6-km bulk and total wind shear values for the LM-only partition are much smaller when compared with those for the LM–RM and RM partitions (compare the Xs with the filled circles in Fig. 2). Based on a one-sided Student's *t*-test for both equal and unequal variances (e.g., Milton and Arnold 1990), the mean 0–6-km bulk and total wind shear values for the LM partition (18.8 and 29.1 m s^{-1}, respectively) were significantly ($\alpha = 0.01$) less than the values for the LM–RM (24.4 and 38.2 m s^{-1}) and RM (24.3 and 39.8 m s^{-1}) partitions. However, there was very little difference in the mean wind shear values between the LM–RM and RM partitions. This suggests that the mean vertical wind shear is significantly weaker in environments that are supportive only of left-moving supercells. Nevertheless, a wide range of shear values does support both left- and right-moving supercells. Therefore, although the bulk and total vertical wind shear provides predictive capability for when supercells might occur (without regard to multicells), it does not effectively discriminate between the environments of left- and right-moving supercells.

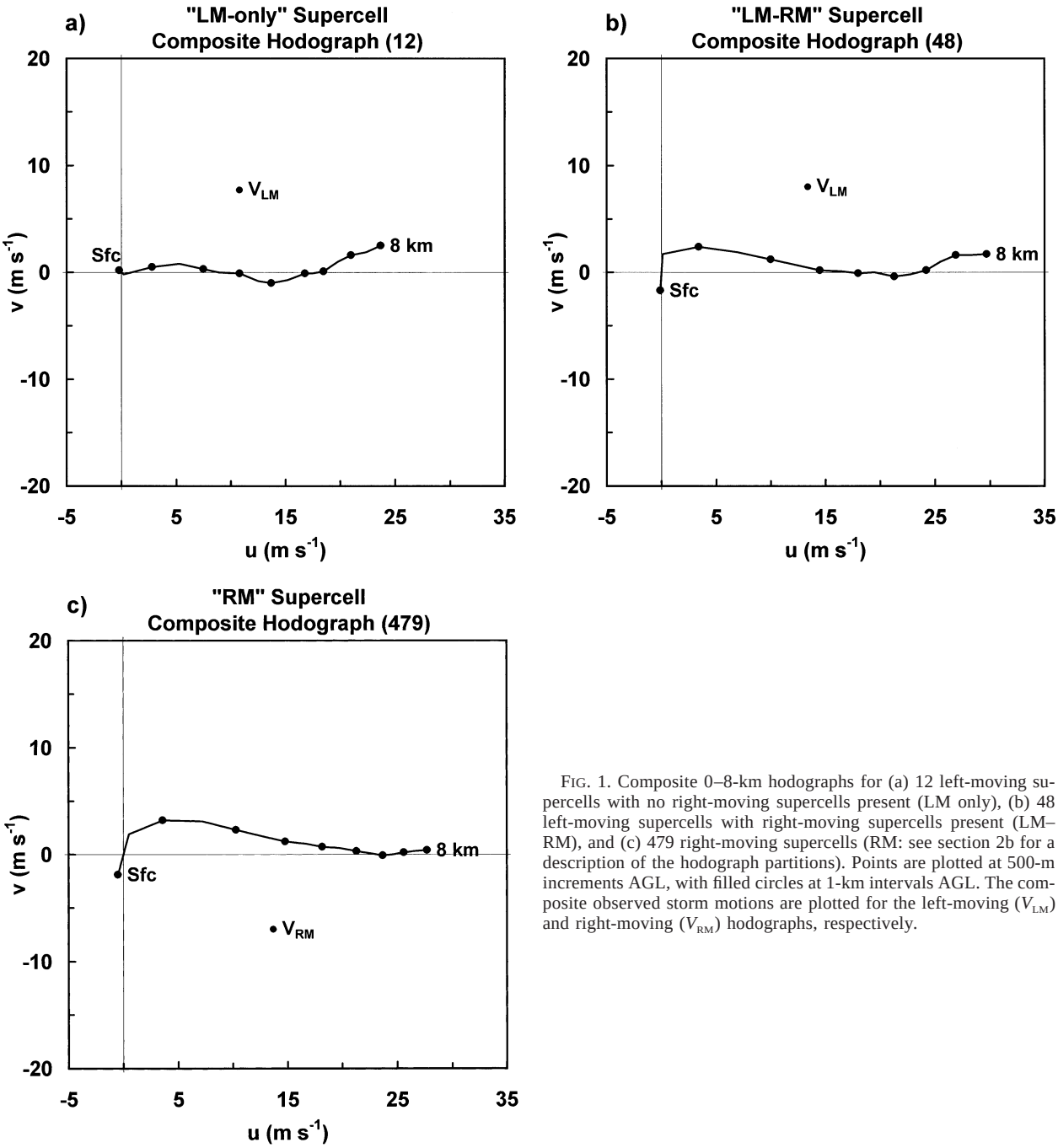

FIG. 1. Composite 0–8-km hodographs for (a) 12 left-moving supercells with no right-moving supercells present (LM only), (b) 48 left-moving supercells with right-moving supercells present (LM–RM), and (c) 479 right-moving supercells (RM: see section 2b for a description of the hodograph partitions). Points are plotted at 500-m increments AGL, with filled circles at 1-km intervals AGL. The composite observed storm motions are plotted for the left-moving (V_{LM}) and right-moving (V_{RM}) hodographs, respectively.

TABLE 2. Total (or cumulative) vertical wind shear, observed SRH, and observed storm-relative flow (SRF) for the LM-only, LM–RM, and RM composite hodographs (see section 2b for a description of the hodograph partitions).

Hodograph partition	0–2-km shear (m s^{-1})	2–8-km shear (m s^{-1})	0–3-km SRH (m^2 s^{-2})	0–1-km SRF (m s^{-1})	8-km SRF (m s^{-1})
LM only	8.0	17.2	−80	12.4	13.9
LM–RM	13.5	20.3	−50	14.2	17.5
RM	14.1	17.7	204	14.9	15.8

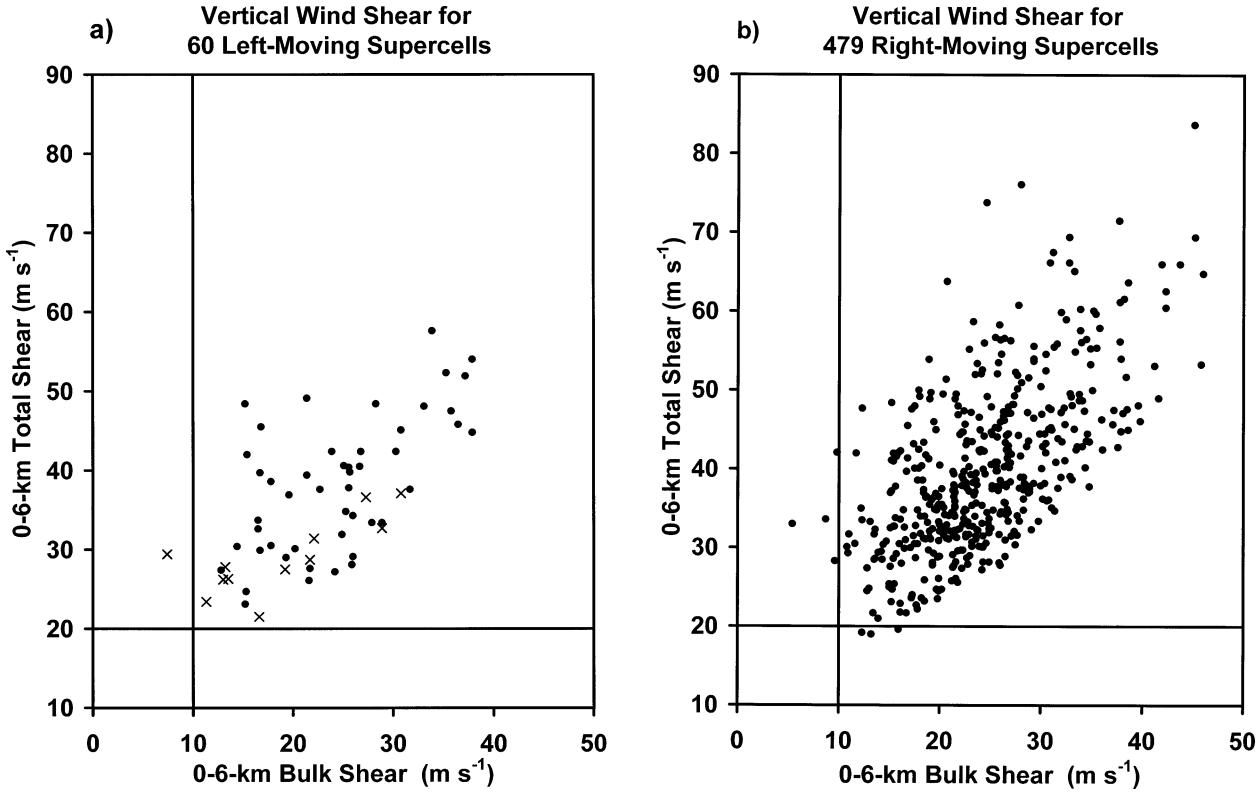

FIG. 2. Observed 0–6-km bulk wind shear plotted against the 0–6-km total wind shear for the (a) 60 left-moving supercells and (b) 479 right-moving supercells. The LM-only dataset is indicated by the Xs (see section 2b for a description of the hodograph partitions).

c. Storm-relative helicity/low-level inflow for supercell environments

Operationally, SRH has often been used as a predictor of supercell occurrence, despite the fact that SRH varies dramatically over small time- and space scales (Markowski et al. 1998b). If SRH had applicability in forecasting the occurrence of right-moving supercells, for example, then one would expect the corresponding SRH values to be significantly positive. However, this author has noted several convective situations where right-moving supercells sometimes occurred for low SRH values. Therefore, in the present study, SRH was investigated to illustrate that deep-layer shear is both more robust and appropriate for anticipating the shear requirements for supercellular convection.

As was expected, there were many instances where the observed 0–3-km SRH magnitude was quite small, despite the occurrence of either left- or right-moving supercells (Fig. 3). If SRH was consistently useful in identifying supercell environments, one would expect the SRH to be significantly negative (positive) for left-moving (right moving) supercells (e.g., Davies-Jones et al. 1990; Droegemeier et al. 1993). However, for the 60 left-moving supercell dataset, the median (modal range) 0–3-km SRH was only -51 m^2 s^{-2} (-100 to -50 m^2 s^{-2}), while for the 479 right-moving supercells, the median (modal range) 0–3-km SRH was 187 m^2 s^{-2} (125–175 m^2 s^{-2}) (Fig. 4, leftmost plots). Furthermore, the 0–3-km SRH was >0 m^2 s^{-2} (<150 m^2 s^{-2}) for more than 25% (33%) of the left-moving (right moving) supercells. This means that either left- or right-moving supercells can occur for observed SRH varying from -40 to 175 m^2 s^{-2}. The main reason for the relatively large percentage of positive 0–3-km SRH values for the left-moving supercells is the clockwise curvature in the lowest 0.5–1 km of the LM–RM hodograph (refer back to Fig. 1b). This is supported by comparing the 0–1-km SRH between the two supercell datasets, where the discriminating value of SRH is even worse (Fig. 4, middle plots); the overlap in the 0–1-km SRH between the left- and right-moving supercells is considerable.

There was some improvement in the utility of SRH when the LM-only partition was compared with the RM partition (compare the Xs with the filled circles in Fig. 3). For the 12 LM-only events, all but one value of 0–3-km SRH was negative, and the median (mean) SRH value was -95 m^2 s^{-2} (-90 m^2 s^{-2}). The difference in SRH between the LM-only and RM partitions was significant ($\alpha = 0.01$), but the difference was not significant between the LM-only and LM–RM partitions. It is important to note that although there were small values of SRH magnitude (-100 to $+100$ m^2 s^{-2}) in 25% of all the cases, this was likely due to the inclusion of cases that had both a left- and right-moving supercell.

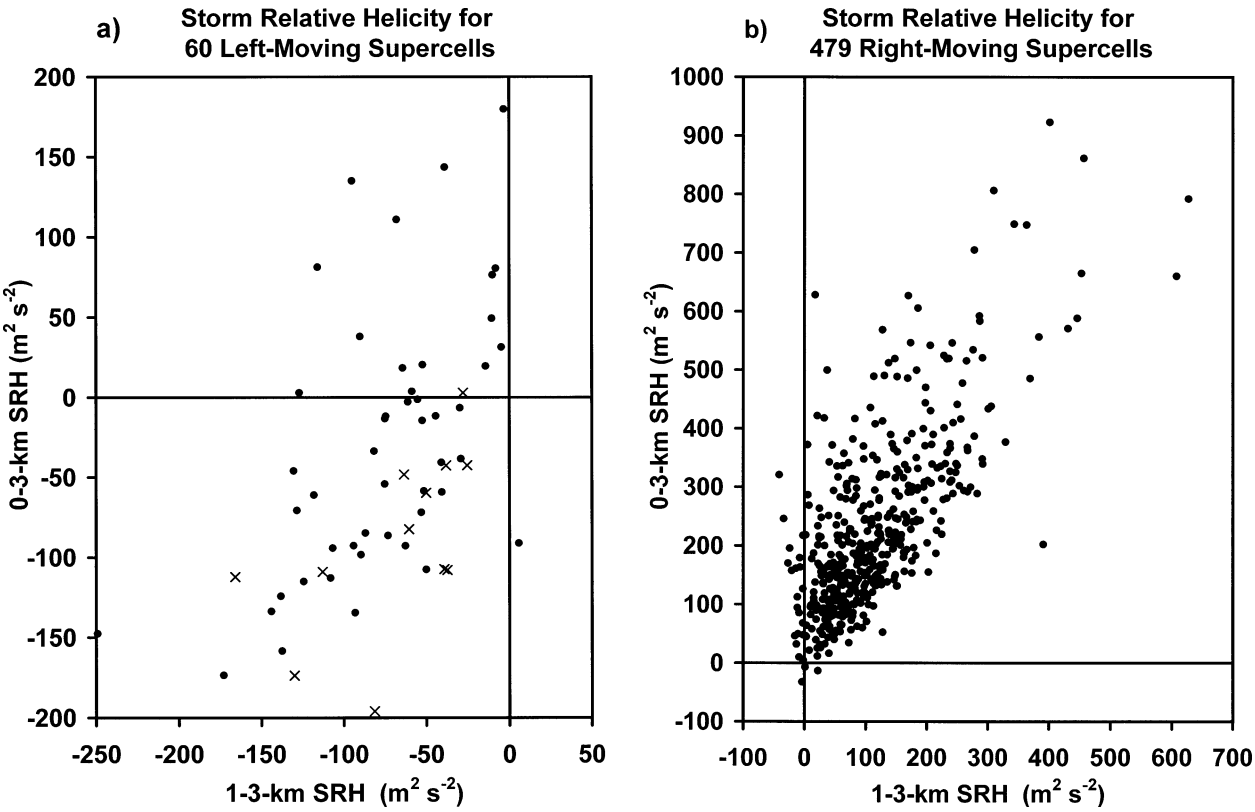

FIG. 3. Observed 1–3-km SRH plotted against the 0–3-km SRH for the (a) 60 left-moving supercells and (b) 479 right-moving supercells. The LM-only dataset is indicated by the Xs (see section 2b for a description of the hodograph partitions).

Such instances, because of geometric arguments, should minimize SRH when the hodograph is unidirectional, which is consistent with the existence of splitting supercells.

After examining the composite hodographs (Fig. 1), it appears that the 1–3-km SRH is a potentially better indicator of left-moving supercells. Accordingly, for all but 1 of the 60 cases, the 1–3-km SRH was negative, with a median value of -64 m^2 s^{-2} (Figs. 3a and 4). Although, in general, the absolute values of SRH for left-moving supercells tend to be much smaller than those for right-moving supercells, absolute values of the 1–3-km SRH are much more comparable between the two datasets, and the overlap is much less noticeable (Fig. 4, rightmost plots). Combined with the 0–3-km SRH, the 1–3-km SRH may have limited potential to discriminate between the environments of supercells that sustain in their rotation after splitting, versus only predominant left- or right-moving supercells.

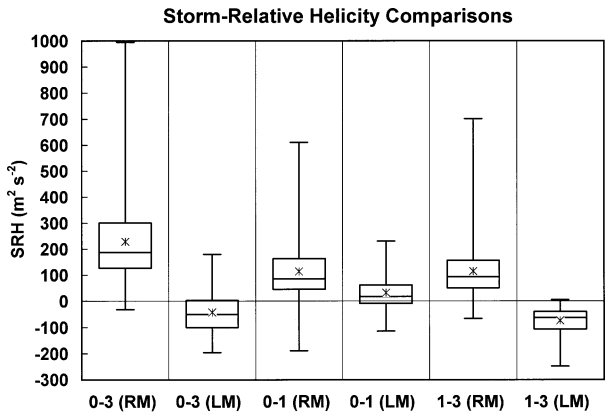

FIG. 4. Box-and-whiskers plots (see Wilks 1995) of observed SRH for the 60 LM vs the 479 RM supercells for the 0–3- (left), 0–1- (center) and 1–3-km (right) layers. The asterisk for each plot represents the mean.

The low-level storm-relative inflow, which is a component of SRH, has also been suggested to be important in maintaining supercells, possibly by preventing the storm outflow from cutting off the moist inflow to the updraft. Davies-Jones et al. (1990) and Droegemeier et al. (1993) suggested that the storm-relative inflow should be $\geq$10 m s^{-1} over the lowest 3 km of the hodograph for sustained supercells. For the present left-moving supercell dataset, the median 0–1-km storm-relative flow was 13.7 m s^{-1}, and it was $>$10 m s^{-1} for 53 of the 60 cases (88%). By way of comparison, the median 0–1-km storm-relative flow was 14.9 m s^{-1} for the 479 right-moving supercells (Table 2). The storm-relative flow was weaker (8 m s^{-1}) in the 2–3-km layer for the LM–RM partition (refer back to Fig. 1b). These

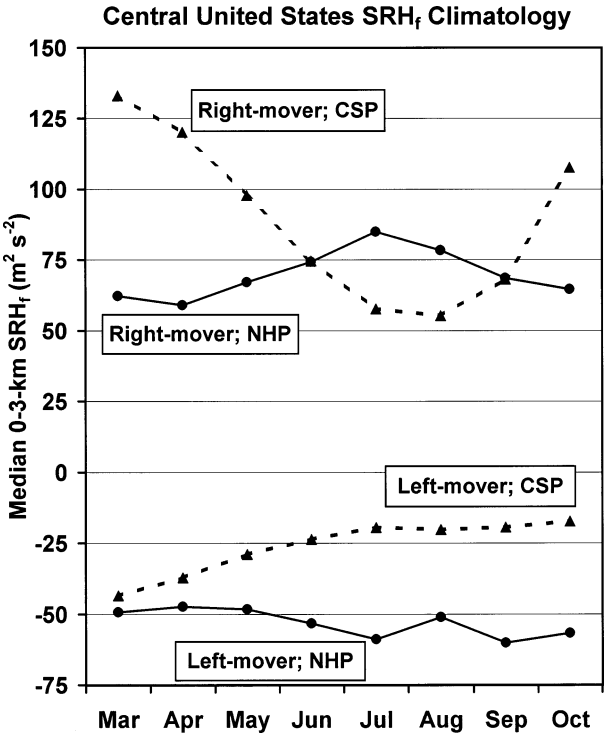

FIG. 5. Median 0–3-km SRH_f by month from 1948 to 2000 for the NHP (represented by Rapid City, SD; Bismarck, ND; Glasgow, MT; Great Falls, MT) and the CSP (represented by Springfield, MO; Topeka, KS; Norman, OK; Fort Worth, TX). Solid (dashed) lines with filled circles (triangles) represent SRH_f for the right- and left-moving supercells across the NHP (CSP). Positive (negative) SRH_f values are for the right-moving (left moving) supercells.

observations are generally consistent with the two studies mentioned above.

d. Climatological analysis of hodographs in the central United States

Nearly 30 000 soundings were analyzed from 1948 to 2000 for the NHP and CSP regions. The range in the number of monthly soundings was from around 250 in March and October for the NHP, to near 4000 in July for the CSP. The period November–February was excluded from the analysis because of the limited number of soundings with significantly positive SBCAPE.

From a climatological perspective, when the SBCAPE is >50 J kg^{-1} and SBCIN is <50 J kg^{-1}, the median 0–3-km SRH_f for right-moving supercells across the CSP is 2–6 times higher than the corresponding SRH_f magnitude for left-moving supercells (Fig. 5; cf. the dashed lines). This ratio is much less over the NHP, ranging from 1.1 to 1.5 times higher SRH_f for right-moving supercells (Fig. 5; cf. the solid lines). The fact that the absolute value of SRH_f is much higher for right-moving supercells than left-moving supercells over the CSP supports the notion that more hodographs exhibit considerable low-level clockwise curvature in this region. Conversely, the much smaller difference in the absolute value of SRH_f between left- and right-moving supercells across the NHP suggests that hodographs tend to be more linear there. Also note that the median values of 0–3-km SRH_f is 120–140 m^2 s^{-2} during the spring season across the CSP; this SRH_f is 35–60 m^2 s^{-2} higher than the peak median values across the NHP. These results are consistent with the timing and relative magnitude of the peak tornado season across the CSP (e.g., Concannon et al. 2000), and also with the climatology of the low-level jet (e.g., Mitchell et al. 1995).

4. Discussion

The primary difference between the kinematic environments of left- and right-moving supercells lies in the lower atmosphere, where clockwise curvature of the hodograph generally occurs over a greater depth for right-moving supercells (Fig. 1c). In environments supporting sustained left- and right-moving supercells after storm splitting, the curvature in the composite hodograph is confined to the lowest 0.5–1 km of the atmosphere (Fig. 1b). Moreover, when only left-moving supercells are considered, the low-level curvature becomes slightly counterclockwise (Fig. 1a). These results are consistent with numerical model simulations, which show that the linear forcing terms lead to preferential development of left-moving (right moving) storms for counterclockwise-curved (clockwise curved) hodographs (Weisman and Rotunno 2000). These findings are also encouraging given both the small sample of LM-only supercells and the difficulties of gathering proximity soundings.

Examples of supercells from numerical model simulations also show that the left-moving supercell becomes weaker, or nonexistent, as clockwise turning of the low-level shear vectors increases from 90° to 180° over an increasingly deeper atmospheric layer, and also as the shear increases in this same layer (e.g., Weisman and Klemp 1986, cf. their Figs. 15.17B and 15.17C; UCAR 1996). This suggests that if the hodograph shear vector turning is shallow (e.g., $<$1–2 km in depth), or if the turning does not exceed 90° in the lowest 3 km, then supercells evolve more like they would in a unidirectionally sheared environment. Of the 60 left-moving supercells in the present study, 46 (77%) had no significant hodograph turning, or the turning was confined only to the lowest 0.5–1 km. In agreement with this, only 12 of the 60 left-moving supercells (20%) were not associated with a right-moving counterpart. Observations of some Australian supercells, where the typical supercell hodograph exhibits only slight counterclockwise turning of the shear vectors through 3 km, also indicate that splitting supercells are fairly common there (Dickins 1994). Furthermore, Houze et al. (1993) reported that left- and right-moving storms were equally common in Switzerland, and not surprisingly, the composite hodographs were nearly unidirectional in the low-

est 3 km. Therefore, left-moving (right moving) supercells will be progressively suppressed as the hodograph displays more clockwise (counterclockwise) turning over a greater depth and angle.

The 0–6-km bulk and total wind shear (in combination) appear to be robust parameters for anticipating the shear requirements for supercells, especially when compared with SRH. This is partly because vertical wind shear is a less volatile parameter than SRH (e.g., Markowski et al. 1998b), and it does not require a storm motion for its computation. Furthermore, updraft–shear considerations appear best at explaining the full range of supercell dynamics (Weisman and Rotunno 2000), which is supported by the similarity/overlap in the 0–6-km shear between the present datasets (Fig. 2). Accordingly, Droegemeier et al. (1993) suggested using the BRN to predict storm type, and to use SRH to estimate supercell rotational potential and storm longevity. It is noted that other layers could have been used to calculate the deep-layer vertical wind shear (e.g., 0–5, 0–7 km), but the present choice appears to be best related to storm motion (e.g., Bunkers et al. 2000).

An unexpected finding is that the deep-layer vertical wind shear was significantly weaker in the environments characterized by only left-moving supercells (i.e., no right-movers present). Stronger vertical wind shears are associated with stronger synoptic-scale systems and, thus, a stronger horizontal temperature gradient. Given the typical vertical wind shear profile in thunderstorm environments across the United States, this would result in a northward component of the left-moving supercell motion, which would often be directed toward the colder, more stable air. Clockwise curvature of the hodograph is also more likely in these environments given the typical presence of the low-level jet. These are possible explanations why left-moving supercells are not as common in the strongest vertical wind shear environments. When the vertical wind shear is weaker, but still sufficient for supercell development, there is a greater likelihood for a more homogeneous air mass on the synoptic scale. This would perhaps lead to more favorable conditions for the persistence of left-moving supercells.

Although SRH has value in predicting the rotational potential of supercells once they have developed (e.g., Droegemeier et al. 1993), and it is a useful tornado forecasting parameter (e.g., Rasmussen and Blanchard 1998), it appears to be a poor predictor of storm type. The fact that small absolute values of SRH have been observed in proximity to supercells makes it an undesirable parameter for predicting the occurrence of ordinary (nontornadic) supercells. A full one-third (two-thirds) of the right-moving supercells in the present dataset were associated with observed 0–3-km SRH $<$ 150 $m^2 s^{-2}$ ($<$250 $m^2 s^{-2}$), which is the rough threshold for mesocyclone development put forth by Davies-Jones et al. (1990) and (Droegemeier et al. 1993). The 0–3-km SRH threshold of 100 $m^2 s^{-2}$ for midlevel mesocyclone development by Stensrud et al. (1997) is more consistent with the observations herein, but even this value is too high in some cases. It is noted that one should be careful when comparing the present datasets (60 left-moving supercells and 479 right-moving supercells, not all tornadic) with the Davies-Jones et al. (1990) dataset (28 tornadic supercells—8 weak, 12 strong, 8 violent); their SRH values are expected to be higher than those for the present dataset because of the association between higher SRH values and tornadic storms (e.g., Rasmussen and Blanchard 1998).

The relative frequency of left-moving supercells across the United States is not well known. Davies-Jones (1986) noted that only 3 of 143 supercells (or 2%) exhibited anticyclonic rotation from 1972 to 1979 in the National Severe Storms Laboratory (NSSL) radar coverage area (i.e., the CSP region). Given the present datasets, one might expect roughly 1 out of every 10 supercells to be a left-mover (e.g., 60/479 = 12%). Several factors explain the low percentage of left-moving supercells studied herein: (i) right-moving supercells have been preferentially documented both in the literature and operationally, and (ii) the WSR-88D does not presently have an operational algorithm to detect left-moving supercells. Additionally, the climatological analysis indicates that this ratio may be geographically biased toward the NHP when compared with the CSP (Fig. 5). It is noted that the 12 LM-only cases were distributed across all parts of the United States, but 5 of them occurred in the NHP. It is also apparent from the climatological SRH_f distribution why left-moving supercells produce relatively less tornadoes across the United States when compared with right-moving supercells (Fig. 5): peak absolute values of SRH_f are higher for right-movers.

This study did not investigate the thermodynamic environments of left-moving supercells. Herein it is presumed that there is a negligible difference between the thermodynamics of left- and right-moving storms, essentially because they both often evolve from a splitting thunderstorm process [e.g., see the discussion on nonlinear forcing in Weisman and Rotunno (2000)], and thus they originate from roughly the same synoptic environment (e.g., McCann 1983). Therefore, the rules of evaluating the atmosphere for moisture, instability, synoptic and mesoscale lift, boundaries, and convective inhibition should be applicable for all supercells. It may be that some left-moving supercells, which originate in a favorable shear environment, do not persist because they travel into a more stable air mass after splitting, (e.g., as they travel well into the cold side of a front). In other cases, left-moving supercells may persist in an unfavorable shear environment because of enhanced low-level convergence along their gust front (e.g., Brown and Meitín 1994). Bluestein and Weisman (2000) suggest that the orientation of the line of forcing with respect to the vertical wind shear vector may also play a role in supercell longevity by modulating adjacent cell

interactions. These are factors that one must consider, in addition to the vertical wind shear parameters presented above, when forecasting supercell occurrence.

5. Conclusions and summary

The following are the conclusions of the present study.

- Hodographs for left-moving supercells across the United States generally exhibit less shear vector turning, shallower turning, or both, in comparison with those for the more dominant right-moving supercells.
- The 0–6-km bulk (total) wind shear is similar between left- and right-moving supercells, with values $>$10–15 m s^{-1} (20–25 m s^{-1}) indicative that supercells are possible (assuming convective initiation).
- When only left-moving supercells occur, deep-layer vertical wind shear is relatively weaker than for right-moving supercell environments, and low-level shear vectors exhibit some counterclockwise curvature.
- SRH is a poorer kinematic parameter than deep-layer vertical wind shear for anticipating *general supercell occurrence* because there is no lower bound like there is for shear, but 1–3-km SRH has some potential value for anticipating left-moving supercells.
- Most left-moving supercells produce severe hail (88% $\geq$ 1.9 cm).

In order to correctly assess the kinematic potential for supercell development, a measure of deep-layer vertical wind shear appears most appropriate. Forecasters should not be surprised when supercells occur in environments characterized by 10–15 m s^{-1} bulk shear and 20–25 m s^{-1} total shear over the lowest 6 km of the hodograph; yet absolute values of SRH are only 40–100 m^2 s^{-2} over the lowest 3 km (environments sometimes considered to be ''weak shear''). BRN takes this deep-layer shear into account (Weisman and Klemp 1986). Left-moving supercells generally occur in environments characterized by unidirectional vertical wind shear, but some clockwise curvature may be present in the lowest 1 km of the hodograph. As clockwise shear vector turning increases from 90° to 180°, or extends through 2–3-km depth, or both, left-moving supercells are progressively less likely, and may need external factors to facilitate their longevity (e.g., McCann 1983; Grasso and Hilgendorf 2001).

SRH has less predictive ability than deep-layer shear in anticipating supercell development, with much overlap in SRH values between left- and right-moving storms. Absolute values of SRH are also typically much lower for left-moving supercells when compared with right-moving supercells. However, the 1–3-km SRH has some potential for anticipating left-moving supercells, with values of -25 m^2 s^{-2} or smaller (i.e., more negative) typically observed. This is a parameter that could easily be derived from operational numerical weather prediction models. In addition, values of 0–3-km SRH for right-moving supercells are often lower than the empirical value of 150 m^2 s^{-2} for supercell development described by Davies-Jones et al. (1990), and much lower than the 250 m^2 s^{-2} threshold in Droegemeier et al. (1993). The current discussion does not apply to tornadic supercells, which do appear to be more strongly associated with positive values of SRH (e.g., Davies-Jones et al. 1990; Rasmussen and Blanchard 1998).

It would be beneficial to implement an operational algorithm for the WSR-88D to detect mesoanticyclones, especially since their parent thunderstorms frequently produce large hail. Monteverdi et al. (2001) presented an example of such an algorithm that was used effectively to detect a left-moving supercell that produced an anticyclonic tornado. If an algorithm similar to this one became operational, it is likely that more left-moving supercells would be recognized in the United States. The algorithm would also greatly assist the operational forecaster when multiple pairs of splitting thunderstorms are present. Moreover, supercell data from the present study, along with a limited climatological analysis of SRH_f, suggest that left-moving supercells may be more common in some areas of the United States than previously thought.

Acknowledgments. I thank Howard Bluestein, Rodger Brown, Don Burgess, Jon Davies, Roger Edwards, Robert Kleyla, John Monteverdi, George Phillips, Richard Thompson, Jon Zeitler, and the Rapid City NWS staff who provided supercell data; Morris Weisman for his helpful discussion on supercell modeling results; David Carpenter, Brian Klimowski, John Monteverdi, Jon Zeitler, and two anonymous persons who reviewed the manuscript; Connie Crandall who obtained some references; and my wife, Heather, who allowed me extra time to work on this manuscript.

REFERENCES

Achtemeier, G. L., 1969: Some observations of splitting thunderstorms over Iowa on August 25–26, 1965. Preprints, *Sixth Conf. on Severe Local Storms,* Chicago, IL, Amer. Meteor. Soc., 89–94.

Andra, D. L., Jr., 1993: Observations of an anticyclonically rotating severe storm. Preprints, *17th Conf. on Severe Local Storms,* St. Louis, MO, Amer. Meteor. Soc., 186–190.

Bluestein, H. B., and M. L. Weisman, 2000: The interaction of numerically simulated supercells initiated along lines. *Mon. Wea. Rev.,* **128,** 3128–3149.

Brown, R. A., 1993: A compositing approach for preserving significant features in atmospheric profiles. *Mon. Wea. Rev.,* **121,** 874–880.

——, and R. J. Meitín, 1994: Evolution and morphology of two splitting thunderstorms with dominant left-moving members. *Mon. Wea. Rev.,* **122,** 2052–2067.

Bunkers, M. J., B. A. Klimowski, J. W. Zeitler, R. L. Thompson, and M. L. Weisman, 2000: Predicting supercell motion using a new hodograph technique. *Wea. Forecasting,* **15,** 61–79.

Burgess, D. W., and E. B. Curran, 1985: The relationship of storm type to environment in Oklahoma on 26 April 1984. Preprints, *14th Conf. on Severe Local Storms,* Indianapolis, IN, Amer. Meteor. Soc., 208–211.

——, and L. R. Lemon, 1991: Characteristics of mesocyclones detected during a NEXRAD test. Preprints, *25th Int. Conf. on Radar Meteorology,* Paris, France, Amer. Meteor. Soc., 39–42.

Charba, J., and Y. Sasaki, 1971: Structure and movement of the severe thunderstorms of 3 April 1964 as revealed from radar and surface mesonetwork data analysis. *J. Meteor. Soc. Japan,* **49,** 191–214.

Concannon, P. R., H. E. Brooks, and C. A. Doswell III, 2000: Climatological risk of strong and violent tornadoes in the United States. Preprints, *Second Conf. on Environmental Applications,* Long Beach, CA, Amer. Meteor. Soc., 212–219.

Davies-Jones, R. P., 1986: Tornado dynamics. *Thunderstorm Morphology and Dynamics,* E. Kessler, Ed., University of Oklahoma Press, 197–236.

——, D. W. Burgess, and M. P. Foster, 1990: Test of helicity as a tornado forecast parameter. Preprints, *16th Conf. on Severe Local Storms,* Kananaskis Park, AB, Canada, Amer. Meteor. Soc., 588–592.

Dickins, J., 1994: South Australian supercells—A composite hodograph. Preprints, *Fourth Severe Thunderstorm Conf.,* Mount Macedon, Victoria, Australia, Bureau of Meteorology, 1–9.

Doswell, C. A., III, and E. N. Rasmussen, 1994: The effect of neglecting the virtual temperature correction on CAPE calculations. *Wea. Forecasting,* **9,** 625–629.

Droegemeier, K. K., S. M. Lazarus, and R. Davies-Jones, 1993: The influence of helicity on numerically simulated convective storms. *Mon. Wea. Rev.*, **121,** 2005–2029.

Edwards, R., and R. L. Thompson, 2000: RUC-2 supercell proximity soundings. Part II: An independent assessment of supercell forecast parameters. Preprints, *20th Conf. on Severe Local Storms,* Orlando, FL, Amer. Meteor. Soc., 435–438.

Fankhauser, J. C., 1971: Thunderstorm–environment interactions determined from aircraft and radar observations. *Mon. Wea. Rev.,* **99,** 171–192.

Grasso, L. D., 2000: The dissipation of a left-moving cell in a severe storm environment. *Mon. Wea. Rev.,* **128,** 2797–2815.

——, and E. R. Hilgendorf, 2001: Observations of a severe left-moving thunderstorm. *Wea. Forecasting,* **16,** 500–511.

Hamill, T. M., and A. T. Church, 2000: Conditional probabilities of significant tornadoes from RUC-2 forecasts. *Wea. Forecasting,* **15,** 461–475.

Hart, J. A., and P. R. Janish, 1999: SeverePlot: Historical Severe Weather Report Database. Version 2.0. Storm Prediction Center, Norman, OK. [Available online at www.spc.noaa.gov/software/svrplot2/index.html.]

Houze, R. A., Jr., W. Schmid, R. G. Fovell, and H.-H. Schiesser, 1993: Hailstorms in Switzerland: Left movers, right movers, and false hooks. *Mon. Wea. Rev.,* **121,** 3345–3370.

Kleyla, R. P., 1993: A radar and synoptic scale analysis of a splitting thunderstorm over north-central Texas on November 10, 1992. Preprints, *17th Conf. on Severe Local Storms,* St. Louis, MO, Amer. Meteor. Soc., 211–214.

Knupp, K. R., and W. R. Cotton, 1982: An intense, quasi-steady thunderstorm over mountainous terrain. Part II: Doppler radar observations of the storm morphological structure. *J. Atmos. Sci.,* **39,** 343–358.

Maddox, R. A., 1976: An evaluation of tornado proximity wind and stability data. *Mon. Wea. Rev.,* **104,** 133–142.

Markowski, P. M., J. M. Straka, and E. N. Rasmussen, 1998a: The sensitivity of storm-relative helicity to small hodograph changes and resolution. Preprints, *19th Conf. on Severe Local Storms,* Minneapolis, MN, Amer. Meteor. Soc., 363–366.

——, ——, ——, and D. O. Blanchard, 1998b: Variability of storm-relative helicity during VORTEX. *Mon. Wea. Rev.,* **126,** 2959–2971.

Matthews, G. N., and T. J. Turnage, 2000: An example of a left-split supercell producing 5-inch hail: The Big Spring, Texas storm of 10 May 1996. Preprints, *20th Conf. on Severe Local Storms,* Orlando, FL, Amer. Meteor. Soc., 526–529.

McCann, D. W., 1983: Synoptic patterns associated with splitting thunderstorms. Preprints, *13th Conf. on Severe Local Storms,* Tulsa, OK, Amer. Meteor. Soc., J1–J4.

Milton, J. S., and J. C. Arnold, 1990: *Introduction to Probability and Statistics: Principles and Applications for Engineering and the Computing Sciences.* McGraw-Hill, 700 pp.

Mitchell, M. J., R. W. Arritt, and K. Labas, 1995: A climatology of the warm season Great Plains low-level jet using wind profiler observations. *Wea. Forecasting,* **10,** 576–591.

Monteverdi, J. P., W. Blier, G. Stumpf, W. Pi, and K. Anderson, 2001: First WSR-88D documentation of an anticyclonic supercell with anticyclonic tornadoes: The Sunnyvale–Los Altos, California, tornadoes of 4 May 1998. *Mon. Wea. Rev.,* **129,** 2805–2814.

Nielsen-Gammon, J. W., and W. L. Read, 1995: Detection and interpretation of left-moving severe thunderstorms using the WSR-88D: A case study. *Wea. Forecasting,* **10,** 127–140.

Phillips, G., 1994: Observation of a left-moving severe thunderstorm. NOAA/NWS CR WSR-88D Operational Note 94-06, 5 pp. [Available from NWS Central Region, 601 E. 12th St., Rm. 1836, Kansas City, MO 64106-2897.]

Rasmussen, E. N., and R. B. Wilhelmson, 1983: Relationships between storm characteristics and 1200 GMT hodographs, low-level shear, and stability. Preprints, *13th Conf. on Severe Local Storms,* Tulsa, OK, Amer. Meteor. Soc., J5–J8.

——, and D. O. Blanchard, 1998: A baseline climatology of sounding-derived supercell and tornado forecast parameters. *Wea. Forecasting,* **13,** 1148–1164.

——, and J. M. Straka, 1998: Variations in supercell morphology. Part I: Observations of the role of upper-level storm-relative flow. *Mon. Wea. Rev.,* **126,** 2406–2421.

Scarlett, J. R., 1998: A severe splitting storm in the upper Yellowstone valley. Preprints, *19th Conf. on Severe Local Storms,* Minneapolis, MN, Amer. Meteor. Soc., 530–531.

Stensrud, D. J., J. V. Cortinas Jr., and H. E. Brooks, 1997: Discriminating between tornadic and nontornadic thunderstorms using mesoscale model output. *Wea. Forecasting,* **12,** 613–632.

Stuart, N. A., 1997: The Wakefield, Virginia WSR-88D depiction of the 6 September 1994 split cell thunderstorm over southern Virginia. *Natl. Wea. Dig.,* **21** (2), 18–30.

Thompson, R. L., and R. Edwards, 2000: A comparison of Rapid Update Cycle 2 (RUC-2) model soundings with observed soundings in supercell environments. Preprints, *20th Conf. on Severe Local Storms,* Orlando, FL, Amer. Meteor. Soc., 551–554.

UCAR, 1996: *A Convective Storm Matrix: Buoyancy/Shear Dependencies.* University Corporation for Atmospheric Research–Cooperative Program for Operational Meteorology, Education, and Training CD-ROM. Version 1.1. [Available from COMET, P.O. Box 3000, Boulder, CO 80307-3000.]

Weaver, J. F., J. F. Dostalek, and L. Phillips, 2001: Left-moving thunderstorms in a high plains, weakly sheared environment. Preprints, *18th Conf. on Weather Analysis and Forecasting,* Fort Lauderdale, FL, Amer. Meteor. Soc., 208–213.

Weisman, M. L., and J. B. Klemp, 1986: Characteristics of isolated convective storms. *Mesoscale Meteorology and Forecasting,* P. S. Ray, Ed., Amer. Meteor. Soc., 331–358.

——, and R. Rotunno, 2000: The use of vertical wind shear versus helicity in interpreting supercell dynamics. *J. Atmos. Sci.,* **57,** 1452–1472.

Wilhelmson, R. B., and J. B. Klemp, 1981: A three-dimensional numerical simulation of splitting severe storms on 3 April 1964. *J. Atmos. Sci.,* **38,** 1581–1600.

Wilks, D. S., 1995: *Statistical Methods in the Atmospheric Sciences.* Academic Press, 467 pp.